

Lingsen Zeng · Jason B. Saleeby · Mihai Ducea

## Geochemical characteristics of crustal anatexis during the formation of migmatite at the Southern Sierra Nevada, California

Received: 6 October 2003 / Accepted: 10 March 2005  
© Springer-Verlag 2005

**Abstract** We provide data on the geochemical and isotopic consequences of nonmodal partial melting of a thick Jurassic pelite unit at mid-crustal levels that produced a migmatite complex in conjunction with the intrusion of part of the southern Sierra Nevada batholith at ca. 100 Ma. Field relations suggest that this pelitic migmatite formed and then abruptly solidified prior to substantial mobilization and escape of its melt products. Hence, this area yields insights into potential mid-crustal level contributions of crustal components into Cordilleran-type batholiths. Major and trace-element analyses in addition to field and petrographic data demonstrate that leucosomes are products of partial melting of the pelitic protolith host. Compared with the metapelites, leucosomes have higher Sr and lower Sm concentrations and lower Rb/Sr ratios. The initial  $^{87}\text{Sr}/^{86}\text{Sr}$  ratios of leucosomes range from 0.7124 to 0.7247, similar to those of the metapelite protoliths (0.7125–0.7221). However, the leucosomes have a much wider range of initial  $\epsilon_{\text{Nd}}$  values, which range from  $-6.0$  to  $-11.0$ , as compared to  $-8.7$  to  $-11.3$  for the metapelites. Sr and Nd isotopic compositions of the leucosomes, migmatites, and metapelites suggest disequilibrium partial melting of the metapelite protolith. Based on their Sr, Nd, and other trace-element characteristics, two groups of leucosomes have been identified. Group A leucosomes have rela-

tively high Rb, Pb, Ba, and  $\text{K}_2\text{O}$  contents, Rb/Sr ratios ( $0.15 < \text{Rb}/\text{Sr} < 1.0$ ), and initial  $\epsilon_{\text{Nd}}$  values. Group B leucosomes have relatively low Rb, Pb, Ba, and  $\text{K}_2\text{O}$  contents, Rb/Sr ratios ( $< 0.15$ ), and initial  $\epsilon_{\text{Nd}}$  values. The low Rb concentrations and Rb/Sr ratios of the group B leucosomes together suggest that partial melting was dominated by water-saturated or  $\text{H}_2\text{O}$ -fluxed melting of quartz + feldspar assemblage with minor involvement of muscovite. Breakdown of quartz and plagioclase with minor contributions from muscovite resulted in low Rb/Sr ratios characterizing both group A and group B leucosomes. In contrast, group A leucosomes have greater contributions from K-feldspar, which is suggested by: (1) their relatively high K concentrations, (2) positive or slightly negative Eu anomalies, and (3) correlation of their Pb and Ba concentrations with  $\text{K}_2\text{O}$  contents. It is also shown that accessory minerals have played a critical role in regulating the partitioning of key trace elements such as Sm, Nd, Nb, and V between melt products and residues during migmatization. The various degrees of parent/daughter fractionations in the Rb–Sr and Sm–Nd isotopic systems as a consequence of nonmodal crustal anatexis would render melt products with distinct isotopic signatures, which could profoundly influence the products of subsequent mixing events. This is not only important for geochemical patterns of intracrustal differentiation, but also a potentially important process in generating crustal-scale as well as individual pluton-scale isotopic heterogeneities.

Communicated by Ian Carmichael

L. Zeng (✉) · J. B. Saleeby  
Division of Geological and Planetary Sciences,  
California Institute of Technology, Pasadena, CA 91125, USA  
E-mail: lzeng@ccsd.org.cn  
Tel.: +86-10-68992875  
Fax: +86-10-68994781

M. Ducea  
Department of Geological Sciences, University of Arizona,  
Tucson, AZ 85721, USA

L. Zeng  
Key Laboratory for Continental Dynamics, MLR,  
Institute of Geology, Chinese Academy of Geological Sciences,  
Beijing 100037, China

### Introduction

The origin of geochemical and isotopic heterogeneities of large granitic batholiths is a fundamental question with regard to granitoid petrogenesis and the evolution of the continental crust (Fyfe 1973; Miller et al. 1988; Sawyer 1998). Heterogeneity in the initial radiogenic isotopic compositions of granitic plutons is commonly

attributed to heterogeneities inherited from source regimes and preserved due to incomplete mixing of the derivative magma. However, contamination of granitic magmas by assimilation of anatectic melts of wallrocks during ascent could also profoundly affect the geochemical and isotopic character of the final products. The role of crustal anatexis at various crustal levels in generating geochemical and isotopic heterogeneities is poorly understood. Thus, characterization of the geochemical and isotopic nature of anatectic melts in high-grade metamorphic terrains would help to better understand the sources of such heterogeneity and their potential magnitude.

Recent experimental and field observations have shown that partial melting at crustal levels is commonly nonmodal (Vielzeuf and Holloway 1988; Le Breton and Thompson 1988; Rushmer 1991; Puziewicz and Johannes 1990; Inger and Harris 1993; Dardien et al. 1995; Harris et al. 1995) and produces melts with isotopic compositions that are in disequilibrium with respect to their sources (Tomomasini and Davies 1997; Knesel and Davidson 2002). Disequilibrium melting refers to any melting event where the liquid phase was not in chemical or isotopic equilibrium with the residue prior to melt extraction. Nonmodal melting is the melting process where the proportion of reactant phases in the source is different from their proportions entering the melt. Crustal anatexis in response to thermal or chemical perturbations is complex, depending on the temperature and pressure conditions, mineral compositions, and water contents. Following a given temperature trajectory and for mica-bearing metasedimentary rocks, melting of quartz and feldspar assemblages is favored by the presence of excessive water and starts at a significantly lower temperature. In contrast, muscovite or biotite dehydration melting reactions occur at a much higher temperature (e.g., Patiño-Douce and Harris 1998). In contrast to muscovite dehydration melting, biotite dehydration melting is more complex because it is continuous over a wide range of temperatures. The temperature at which this reaction occurs depends on the composition of biotite (Mg/Fe ratio, Ti and F concentration) and the bulk Al content of source rocks (Le Breton and Thompson 1988; Vielzeuf and Montel 1994; Patiño-Douce and Beard 1996; Stevens et al. 1997; Nabelek and Bartlett 2000).

In this paper, we report the results of a detailed field and geochemical study of a well-developed migmatite zone in the Isabella pendant of the southern Sierra Nevada batholith in California. This migmatite zone is of particular interest because it represents a single prograde metamorphic sequence from greenschist facies metasediments to migmatites that lie in direct contact with the ca. 100 Ma Goat Ranch granodiorite pluton of the composite batholith. Field relations suggest that this pelitic migmatite zone formed and then abruptly solidified prior to substantial mobilization and escape of its melting products. Hence, this area yields important insights into potential mid-crustal level contributions of crustal com-

ponents into Cordilleran-type batholiths. In this paper, we intend to address (1) the geochemical nature of the melting products from the metapelite, (2) the magnitude of isotopic heterogeneity produced by such crustal anatexis, (3) elemental and isotopic fractionations associated with the formation of the migmatites, and (4) implications for the intracrustal differentiation and isotopic heterogeneities within Cordilleran-type batholiths. The nomenclature used in this paper follows that of Johannes (1988). Leucosome is the leucogranitic portion formed during migmatization, and the melanosome is the mafic-rich selvage between the leucosome and mesosome. Mesosome has intermediate color between the leucosome and melanosome in a migmatite and differentiates into leucosome and melanosome during migmatization. The rock undergoing migmatization is called the parent rock, which in the nonmigmatitic far field is also referred to as the protolith.

---

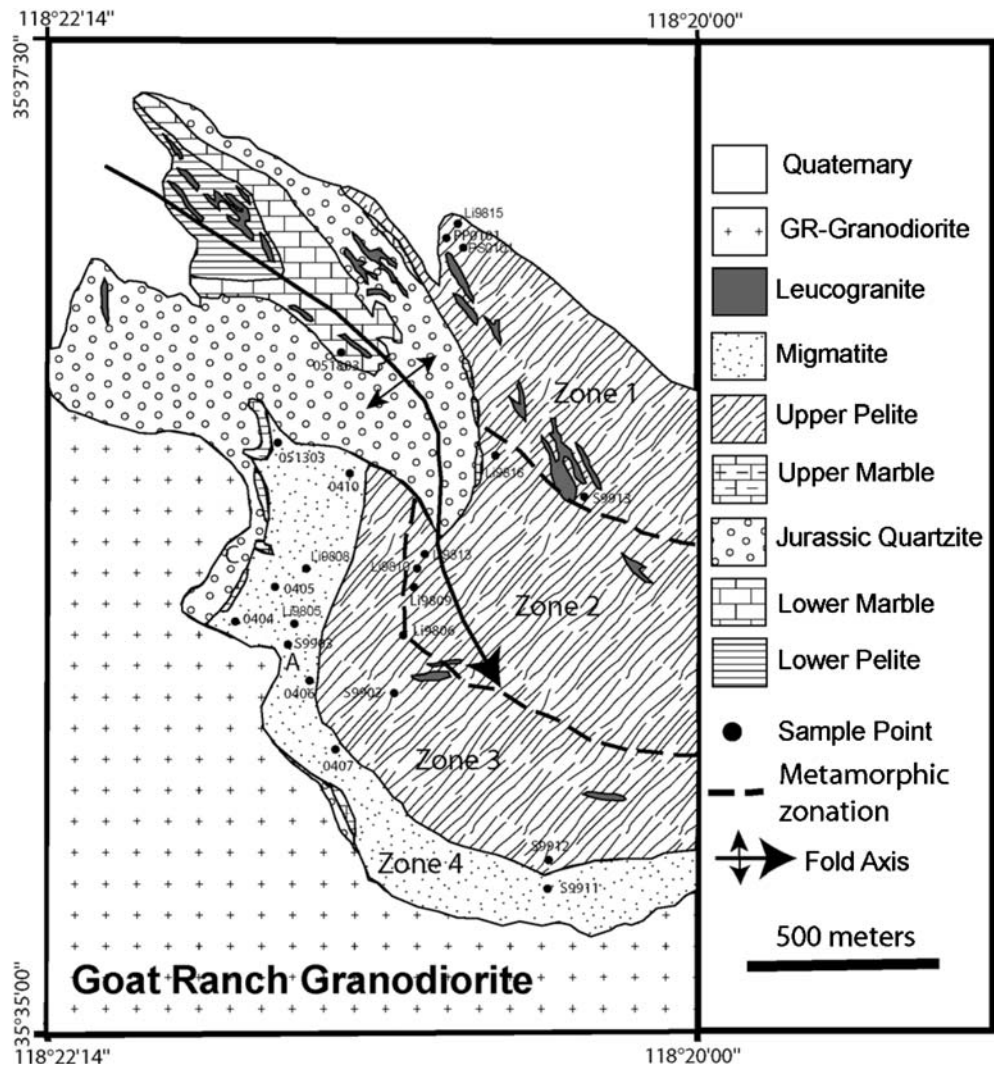
## Geologic setting

Metamorphic rocks of the Isabella pendant consist of a stratified sequence of pelitic and psammitic schist and gneiss, quartzite, marble, and calc-silicate rock. This sequence of stratified rocks constitutes one of the best preserved sections through the early Mesozoic Kings sequence, which constitutes a distinct family of pendants that runs for over 250 km along the axis of the southern Sierra Nevada batholith (Saleeby and Bushy 1993). The entire pendant reached amphibolite facies conditions during emplacement of and engulfment by the late Cretaceous plutons. U/Pb zircon ages indicate the emplacement of these plutons in the  $100 \pm 2$  Ma time interval (Saleeby and Zeng 2005).

A geologic map of the area that was studied in detail within the Isabella pendant is shown in Fig. 1. The structure is characterized by a steeply SE-plunging isoclinal anticline with pelite units situated in core and envelope positions of the fold. Metamorphic fabrics associated with the fold are L-S with the linear element parallel to steeply plunging fold axes. Finite strain studies on deformed pebble conglomerate in the quartzite unit indicate a stretch factor up to  $\sim 1,000\%$  along the steep lineations. Homoaxial deformation in satellite dikes from the Goat Ranch intrusion and leucosomes of the migmatitic pelite, as well as peak metamorphic textures, indicate that the isoclinal folding and L-S fabric development occurred during pluton emplacement.

The upper pelite unit (J-pelite), which envelopes the large fold and is in contact with the Goat Ranch intrusion, has an apparent stratigraphic thickness in excess of 1 km. Remnants of primary structures in the lowest metamorphic grade areas suggest a protolith of thin bedded compositionally immature turbidite. The protolith was remarkably homogenous in lithologic composition and in primary structure. Except for subordinate

**Fig. 1** Geologic map of the Isabella pendant at the south Lake Isabella area and adjacent Goat Ranch granodiorite intrusion showing the distribution of migmatitic zone and tentative metamorphic zonation within the Jurassic pelite unit



psammitic layers, the notable lithologic variation through the entire unit results from a metamorphic gradient, which roughly extends normal to the axial surface of the large fold and into the proximal contact zone with the Goat Ranch intrusion. Based on the mineral assemblages, we can define metamorphic zones with proximity to the Goat Ranch granodiorite. The zones (Fig. 1) consist of: (1) distal muscovite-bearing biotite–andalusite schist (about 5% muscovite), (2) biotite–andalusite co-existing with sillimanite–microcline schist with incipient granitic leucosomes, (3) biotite–sillimanite–microcline schist with local granitic leucosomes, and (4) sillimanite–microcline schist with significant or extensive leucosomes.

### High-grade pelites and migmatites

Migmatitic metamorphic zones occur at several localities that are in close proximity to batholithic contacts within the Kings Sequence pelites of the Lake Isabella region. The migmatite zone shown in Fig. 1 is the most exten-

sive of these and can be related to a very well-defined metamorphic gradient through the upper pelite unit (J-pelite). This pelite unit has a relatively uniform and stratigraphically thick protolith sequence, and its transition from its migmatite zone into the xenolithic marginal phase of the Goat Ranch intrusion is well exposed. This area was originally studied by Best and Weiss (1964) who designated the rocks as "hornfels", therefore envisioning metamorphism and migmatization as pluton emplacement-related. Except for granoblastic textures in the migmatite leucosomes, the metamorphic textures are penetratively schistose and/or gneissose and reflect a high degree of plastic strain during plutonism and metamorphism (Saleeby and Busby 1993). Swarms of felsic dikes that are distinct from the migmatitic leucosomes cut each stratigraphic unit of the pendant, and exhibit high ductile strain features that are co-axial with the isoclinal folding event and developed during their intrusion. These dikes also yield U/Pb zircon ages in the  $100 \pm 2$  Ma range (Saleeby and Zeng 2005), which along with the meso- and map-scale relations between the migmatite and Goat Ranch pluton indicate that

migmatization and high-magnitude strain resulted from batholith emplacement. The leucosomes that developed during migmatization can be morphologically divided into: (1) concordant (stromatitic) and pervasive network leucosomes (Fig. 2a and b), (2) discordant dikes and pockets of pegmatites and aplites (Fig. 2d), and (3) agmatitic and randomly distributed leucosome patches of various sizes, which appear to represent the gathering of quartzo-feldspathic segregations into larger, granitic-, or pegmatitic tubes and dikes. There are also very finely laminated migmatites, which have stromatitic or pervasive network structures such as those shown in Fig. 2a. Such finely laminated migmatitic textures and structures pervade much of the matrix of the migmatite complex including the residue-rich domains from which larger-scale leucosomes have segregated. Finely laminated migmatites occur in two field settings: (1) large (10's m<sup>2</sup>) domains with no apparent segregation of thickened ( $\geq$ cm-scale) leucosomes; and (2) domains where such thickened leucosomes lie within a host of the finely laminated migmatites. True melanosomes, or pure residue layers, are restricted to sub-millimeter-scale lamina of predominantly biotite with subordinate sillimanite, felsic minerals, opaque minerals, and rare garnet. The extremely fine scale with typical one to two mineral grain thicknesses prohibits the pure separation and analysis of such melanosomes. We will return to this problem below.

Nonmigmatitic metapelite in Zone 1 (Fig. 1) consists of andalusite, biotite, quartz, K-feldspar, plagioclase, muscovite (<5%), and minor sillimanite. The leucosomes associated with the finely laminated migmatite mainly consist of quartz, K-feldspar, and plagioclase, and have a granoblastic texture. Generally, quartz, K-feldspar, and plagioclase in the leucosomes are substantially coarser than those in the mesosomes or melanosomes. In thin sections, some of the leucosomes have

trace amounts of apatite located at the boundaries of quartz and plagioclase, which suggests relatively high levels of P<sub>2</sub>O<sub>5</sub> in such leucosomes. In contrast, the melanosomes mainly consist of biotite (up to 60%) and sillimanite with subordinate quartz, plagioclase, and K-feldspar. Garnets co-existing with biotites are rarely found within the migmatite zone. They are found in only two localities that are in proximity to the Goat Ranch pluton throughout the entire study area.

The pressures at which the presently exposed Sierra Nevada batholith was emplaced gradually increase southward from 2 kb at latitude 37°45'N, to ~9 kb at the extreme southern end of the batholith (Ague and Brimhall 1987; Pickett and Saleeby 1993; Ague 1997). In this studied area, the Goat Ranch pluton was emplaced at a pressure between 3 and 5 kb (Dixon 1995) and at a temperature of ~700 °C (Elan 1985). The presence of andalusite coexisting with biotite in the upper pelitic unit suggests a temperature as low as ~450 °C at 1.5 km from the Goat Ranch intrusion. Elan (1985) has studied the *P-T* conditions of thermal metamorphism of the Isabella pendant that is in direct contact with the Cyrus Flat pluton in the north shore area of the Isabella pendant ~5 km north of the study area. His results show that the temperature at the contact between the Isabella pendant and Cyrus Flat pluton was about 730 °C, declining to ~430–475 °C at the margin of the aureole ~2 km from the contact, and the Cyrus Flat pluton was emplaced at a pressure about 3 kb. Because of the structural continuity throughout the entire Isabella pendant, similarity in metamorphic assemblages of the metasedimentary rocks studied by Elan (1985) to those of this study area, and the same age of the Goat Ranch and Cyrus Flat plutons (Saleeby and Zeng 2005), the *P-T* conditions determined by Elan (1985) appear to be applicable to the study area. Thermobarometric studies by Pickett and Saleeby (1993) carried out on a small

**Fig. 2** Structures of the migmatites showing **a** photomicrograph of stromatitic structure, **b** field photography of anastomose structure, **c** field photograph of chaotic structure, and **d** field photograph of melt pockets along the fracture zone

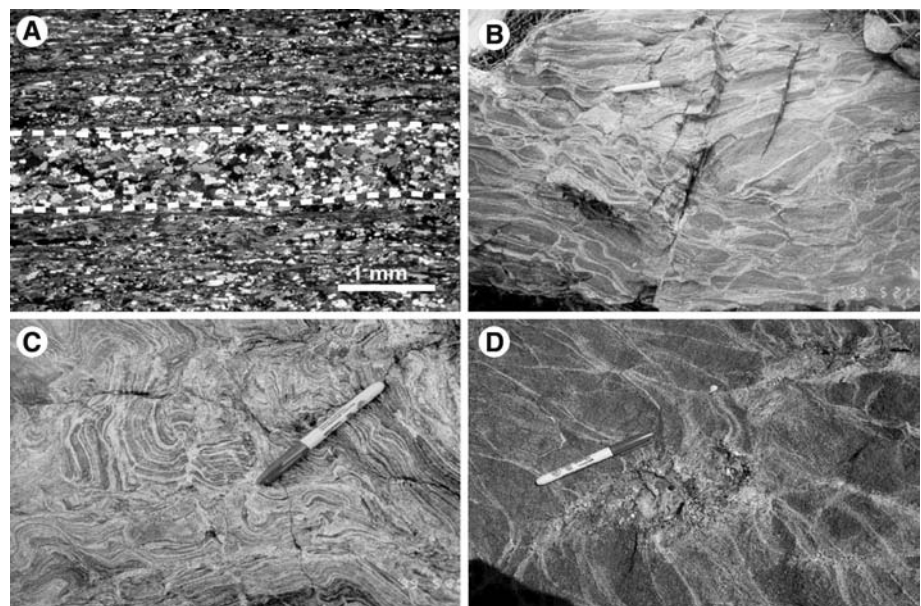


**Table 1** Major and trace-element analytical results for selected samples of metapelite, migmatite, and leucosome

	PP0101 Metapelite	PS0101 Metapelite	Li9815 Metapelite	Li9805 Migmatite	Li9808 Migmatite	R0410 Migmatite*	R0407 Migmatite*	R0404 Migmatite*	L0404 Leucosome	L0405 Leucosome	L0407 Leucosome	L0410 Leucosome
Major element (wt%)												
SiO <sub>2</sub>	63.08	64.95	63.01	67.94	68.73	63.94	62.07	69.74	80.91	74.97	75.67	69.59
Al <sub>2</sub> O <sub>3</sub>	23.17	23.42	21.52	18.11	17.53	20.54	20.04	16.23	14.48	16.99	14.58	17.41
TiO <sub>2</sub>	0.986	0.926	0.866	0.828	0.851	0.978	1.021	0.616	0.086	0.381	0.047	0.514
FeO	6.10	4.94	6.82	5.45	4.86	5.70	7.26	5.57	0.86	1.85	0.76	3.78
MnO	0.047	0.032	0.043	0.078	0.143	0.083	0.109	0.080	0.033	0.054	0.013	0.066
CaO	0.25	0.22	0.25	0.76	0.70	0.64	0.76	1.03	0.54	1.64	0.95	0.61
MgO	1.64	1.59	2.09	1.82	1.40	1.49	2.16	1.36	0.18	0.54	0.14	1.00
K <sub>2</sub> O	2.52	1.82	2.83	2.25	2.33	3.10	3.52	2.23	0.36	0.47	4.59	3.68
Na <sub>2</sub> O	0.84	0.54	0.39	0.90	1.19	1.74	1.47	1.42	0.72	2.06	2.13	1.89
P <sub>2</sub> O <sub>5</sub>	0.183	0.083	0.324	0.182	0.161	0.144	0.115	0.173	0.083	0.112	0.129	0.143
Total	98.81	98.52	98.14	98.31	97.90	98.35	98.53	98.45	98.25	99.06	99.01	98.68
Trace elements (ppm)												
Ni	35	41	33	35	35	35	38	22	13	14	8	22
Cr	106	123	93	76	77	88	92	46	11	17	3	41
Sc	23	21	20	27	11	26	29	14	2	4	0	14
V	127	168	139	114	112	131	136	77	22	40	4	64
Ba	463	499	521	555	1032	802	636	364	121	193	1116	875
Rb	186	115	164	125	97	167	184	115	14	17	138	131
Sr	102	65	119	156	148	215	186	426	229	269	302	230
Zr	190	166	167	225	254	193	227	179	69	188	82	116
Y	37	33	35	35	37	38	41	28	21	33	35	36
Nb	18.8	18.9	19.2	20.2	17.2	22.2	24.8	14.8	4.0	9.1	2.6	13.3
Ga	26	28	25	21	22	26	26	16	18	20	15	18
Cu	12	0	8	0	11	0	0	27	4	0	1	0
Zn	74	80	111	85	75	77	94	67	8	21	6	49
Pb	16	25	16	21	30	43	32	36	13	29	44	48
Th	17	16	14	16	19	16	18	15	5	18	12	17
Rare Earth element (ppm)												
La	50.52	49.46	45.31	40.88	48.54	47.88	48.01	34.91	13.88	39.01	20.15	32.17
Ce	65.25	61.53	58.46	54.51	64.73	63.13	64.45	45.91	18.45	50.82	26.72	42.66
Pr	10.7	10.19	9.42	8.77	10.18	10.12	10.37	7.38	3.01	8.06	4.33	6.9
Nd	41.42	38.81	36.63	34.84	39.63	39.81	40.43	29.75	11.92	30.68	16.74	26.67
Sm	9.03	8.1	7.98	7.77	8.78	8.74	8.95	6.93	3.07	6.7	4.22	6.26
Eu	1.27	1.14	1.07	0.82	1.24	1.78	1.29	1.00	0.43	1.28	1.83	1.76
Gd	7.51	6.29	6.96	6.73	7.36	7.36	7.59	6.5	3.2	5.79	4.24	5.67
Tb	1.2	1.01	1.15	1.11	1.17	1.16	1.21	1.02	0.57	0.96	0.88	1.01
Dy	7.13	6.13	6.8	6.73	6.84	6.72	7.11	5.66	3.58	5.83	6.02	6.37
Ho	1.43	1.27	1.36	1.34	1.39	1.32	1.43	1.08	0.73	1.19	1.35	1.34
Er	3.84	3.49	3.68	3.73	3.69	3.6	3.94	2.83	2.12	3.31	4.03	3.81
Tm	0.58	0.52	0.54	0.55	0.55	0.51	0.58	0.4	0.35	0.5	0.63	0.59
Yb	3.62	3.35	3.42	3.42	3.53	3.26	3.68	2.47	2.28	3.06	4.14	3.67
Lu	0.58	0.53	0.53	0.54	0.55	0.51	0.58	0.38	0.37	0.49	0.66	0.58

metasedimentary pendant to the south of the study area yielded peak metamorphic conditions of 10.8 kb and 788 °C. Because the metasedimentary rocks in the present study were located at a much higher crustal level than those studied by Pickett and Saleeby (1993), thermal conditions resolved by these workers are taken as an upper bound for the Goat Ranch granodiorite and its proximal thermal aureole.

The common occurrence of leucogranite dikes with primary tourmalines and skarn deposits within calcareous units suggests intensive hydrothermal activity during high-grade metamorphism and the formation of the migmatite complex. The implied elevated fluid activity might have lowered the solidus and promoted partial melting of quartz + feldspar assemblage, while it inhibited muscovite dehydration melting (Patiño-Douce and Harris 1998).

### Analytical techniques

We have carried out major, trace element, and Sr–Nd isotopic analyses on a suite of leucosomes and their proximal hosts, finely laminated migmatites, and metapelites from the Isabella pendant. Migmatites containing thickened leucosomes ( $\geq$ cm-scale) were selected for separation of leucosomes for major, trace, and Sr–Nd isotopic analysis. We refer to such migmatite after extraction of the thickened leucosomes (<5%) as proximal hosts for leucosomes. Separation of leucosomes was done by (1) careful examination of migmatites (of a size 10×15×5 cm) containing thickened leucosomes; (2) cutting thicken leucosomes from the migmatite; (3) hand-picking and washing leucosomes

with purified water to ensure least contamination from mafic selvages; (4) letting the leucosomes dry for 72 h, and then (5) using a tungsten carbide shatter box to prepare the powder for each sample. For migmatites and metapelites, representative samples were prepared by following the similar procedures to those of leucosomes, except that each sample has a size bigger than 15×15×5 cm. Bulk-rock major, trace, and rare earth element concentrations were obtained by X-ray fluorescence and ICP-MS at the Department of Geology, Washington State University. Procedures and reproducibility are reported in Johnson et al. (1999). Bulk-rock major and trace-element data are listed in Table 1. We have conducted Sr and Nd bulk-rock isotopic studies to characterize the isotopic compositions and test for homogeneity versus heterogeneity of the metapelites, leucosomes, proximal hosts, and finely laminated migmatites. The analytical techniques are described in Pickett and Saleeby (1994) and Ducea and Saleeby (1998). The Nd and Sr measurements were corrected for mass fractionation by normalization to  $^{146}\text{Nd}/^{142}\text{Nd}=0.63615$ , and  $^{87}\text{Sr}/^{86}\text{Sr}=0.1194$ . External precisions during this period of measurement for Sr and Nd isotopic compositions are  $\pm 0.000016$  ( $n=18$ ), and  $\pm 0.000019$  ( $n=18$ ), respectively.  $^{87}\text{Sr}/^{86}\text{Sr}$  for the NBS987 standard is 0.710252 and  $^{143}\text{Nd}/^{144}\text{Nd}$  for La Jolla Nd standard 0.5118587. The analytical results are given in Table 2. Initial Sr and Nd ratios were corrected back to 100 Ma, which is the emplacement age of the Goat Ranch and adjacent plutons, and the timing of peak metamorphism and deformation of the Isabella pendant (Saleeby and Zeng 2005). In the following sections, the symbol sizes in all the plots are larger than the analytical errors.

**Table 2** Nd and Sr isotopic compositions of the metapelite protoliths, migmatites, and leucosomes

Sample	Rock-type	Rb (ppm)	Sr (ppm)	$^{87}\text{Rb}/^{86}\text{Sr}$	$^{87}\text{Sr}/^{86}\text{Sr}$	$^{87}\text{Sr}/^{86}\text{Sr}$ (100)	Sm (ppm)	Nd (ppm)	$^{147}\text{Sm}/^{144}\text{Nd}$	$^{143}\text{Nd}/^{144}\text{Nd}$	$\epsilon_{\text{Nd}}$ (100) <sup>b</sup>	Eu/Eu* <sup>a</sup>
PP0101	Metapelite	175.65	103.56	4.8844	0.722352	0.715412	8.96	42.66	0.1270	0.512118	-9.26	0.478
PS0101	Metapelite	108.39	69.21	4.5123	0.728495	0.722083	8.06	41.11	0.1185	0.512081	-9.87	0.496
Li9805	Migmatite	123.31	158.54	2.2375	0.716645	0.713465	8.37	47.52	0.1064	0.512143	-8.50	N/A
Li9808	Migmatite	90.80	137.32	1.9022	0.716636	0.713932	7.83	42.89	0.1103	0.512142	-8.57	0.353
Li9810	Metapelite	153.10	247.20	1.7831	0.718446	0.715912	9.51	52.30	0.1100	0.512088	-9.62	0.476
Li9813	Metapelite	88.00	92.30	2.7484	0.721861	0.717956	4.89	26.48	0.1171	0.512137	-8.69	N/A
Li9815	Metapelite	163.70	143.70	3.2790	0.717148	0.712489	7.48	47.72	0.0947	0.511992	-11.31	0.442
Li9816	Metapelite	172.10	57.20	8.6757	0.729700	0.717372	8.20	47.39	0.1046	0.512056	-10.19	N/A
R0410	PH	163.63	224.41	2.0987	0.718356	0.715378	5.84	29.05	0.1216	0.512123	-9.10	0.685
R0406	PH	168.18	370.00	1.3086	0.719961	0.718101	7.55	36.30	0.1257	0.512107	-9.46	N/A
R0407	PH	177.11	193.36	2.6375	0.722111	0.718364	5.63	37.02	0.0919	0.512106	-9.04	0.483
R0404	PH	105.81	471.06	0.6464	0.717761	0.716843	6.83	21.13	0.1955	0.512129	-9.91	0.462
L0404	Leucosome	12.34	267.17	0.1394	0.712585	0.712397	1.63	10.45	0.0939	0.512006	-11.03	0.421
L0405	Leucosome	15.46	260.32	0.1709	0.714695	0.714452	3.08	27.69	0.0670	0.512009	-10.62	0.635
L0406	Leucosome	101.26	675.07	0.4286	0.716931	0.716322	2.99	10.31	0.1745	0.512291	-6.50	N/A
L0407	Leucosome	134.58	311.01	1.2469	0.717532	0.715761	3.39	10.22	0.1996	0.512334	-5.98	1.341
L0410	Leucosome	126.13	263.71	1.3780	0.726609	0.724651	6.26	27.01	0.1395	0.512243	-6.98	0.915
051803	Marble	1.02	383.32	0.0077	0.711327	0.711317	0.05	0.26	0.1216	0.512417	-3.35	N/A

<sup>a</sup>Eu anomaly is calculated by  $\text{Eu}/\text{Eu}^* = \text{Eu}_N / \sqrt{\text{Sm}_N \times \text{Gd}_N}$ , where  $\text{Eu}_N$ ,  $\text{Sm}_N$ , and  $\text{Gd}_N$  are normalized to chondrite (Sun and McDonough 1989). PH Proximal host for leucosomes

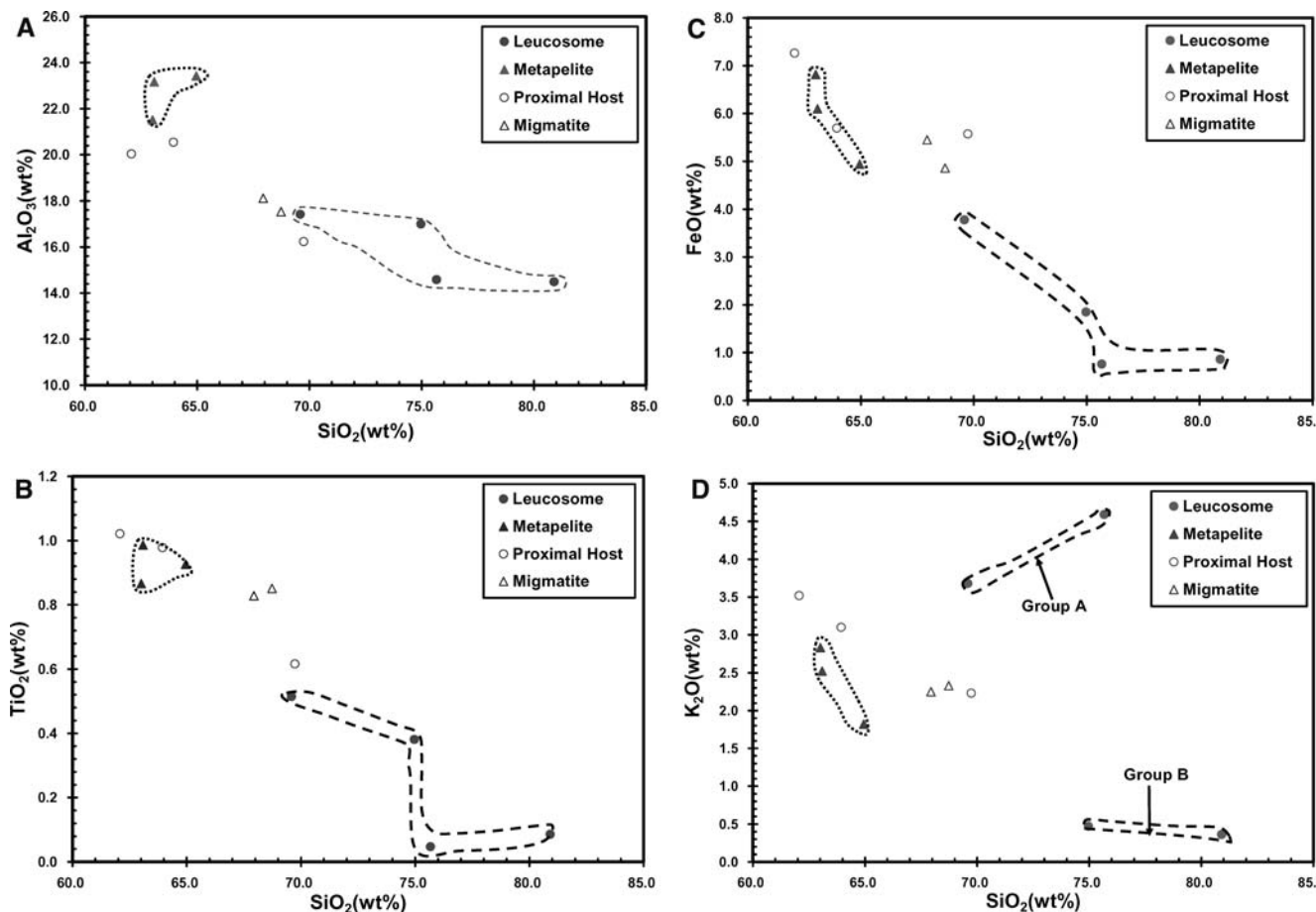
<sup>b</sup>Calculated at  $t=100$  Ma using the equation  $\epsilon_{\text{Nd}}(t) = \left[ \frac{(^{143}\text{Nd}/^{144}\text{Nd})_{\text{sample}}(t)}{(^{143}\text{Nd}/^{144}\text{Nd})_{\text{CHUR}}(t)} - 1 \right] \times 10^4$ , and  $(^{143}\text{Nd}/^{144}\text{Nd})_{\text{CHUR}}(0) = 0.512635$  and  $(^{147}\text{Sm}/^{144}\text{Nd})_{\text{CHUR}}(0) = 0.1966$

## Major and trace-element geochemistry

Major and trace-element data are listed in Table 1. Metapelites, migmatites (including the proximal host for leucosome and the finely laminated migmatite), and leucosomes can be distinguished in their major element compositions. The metapelites have higher  $\text{Al}_2\text{O}_3$ ,  $\text{TiO}_2$ ,  $\text{FeO}$ , and  $\text{MgO}$ , but lower  $\text{MnO}$  and  $\text{CaO}$  contents than those in the migmatites and leucosomes. In general, the leucosomes have higher  $\text{SiO}_2$  contents than both the migmatites, and metapelites. Selected major element variations for the leucosomes, migmatites and metapelites are illustrated in Fig. 3. The metapelites have limited ranges of  $\text{SiO}_2$  from 63.0 to 65.0, when compared to relatively greater variations of  $\text{SiO}_2$  contents in the migmatites. Leucosomes have lower  $\text{FeO} + \text{MgO}/\text{Al}_2\text{O}_3$  ratios ( $< 0.274$ ) than those of both the migmatites and

metapelites ( $> 0.279$ ). As shown in Fig. 3,  $\text{Al}_2\text{O}_3$ ,  $\text{TiO}_2$ ,  $\text{MgO}$ , and  $\text{FeO}$  are negatively correlated with  $\text{SiO}_2$  in the metapelites, migmatites and leucosomes, which suggests that their major element geochemistry is dominantly controlled by constituent phases involved in the partial melting. Preferential melting of quartz, K-feldspar, and/or plagioclase from a pelitic source will lead to elevated  $\text{SiO}_2$  but decreased  $\text{FeO}$ ,  $\text{MgO}$ ,  $\text{TiO}_2$ , and  $\text{Al}_2\text{O}_3$  contents in the leucosome (Fig. 3c). Due to limited volume of leucosomes ( $< 5\%$ ) extracted for analyses, the complimentary proximal host samples have similar major element compositions to those of the finely laminated migmatites (Fig. 3a, b and c). Both the proximal hosts and migmatites have lower  $\text{Al}_2\text{O}_3$  contents than those in the metapelites. This may be due to protolith variations towards psammitic compositions expressed mineralogically by a nonuniform distribution of sillimanite. Based on their  $\text{K}_2\text{O}$  contents (Fig. 3d), the leucosomes can be subdivided into two groups: high-K group A and low-K group B. Group A samples have  $\text{K}_2\text{O}$  contents of 3.68 and 4.59 wt%, while group B samples have much lower  $\text{K}_2\text{O}$  content of 0.36 and 0.49 wt%. We have calculated the CIPW norm of those leucosomes with major element geochemistry data and plotted them on an Ab–An–Or ternary diagram (Fig. 4). This diagram (Fig. 4) also shows the composition data of melts from experimental partial melting of muscovite schist (MS) and muscovite–

**Fig. 3** Selected major element oxides versus  $\text{SiO}_2$  diagram for selected leucosomes, migmatites (including proximal host for leucosome and migmatite), and metapelites. Diagrams showing the relationships between **a**  $\text{Al}_2\text{O}_3$ , **b**  $\text{TiO}_2$ , **c**  $\text{FeO}$ , and **d**  $\text{K}_2\text{O}$  with  $\text{SiO}_2$  (wt%). The term “proximal host for leucosome” refers to the material after the separation of relatively large size of leucosomes from a finely laminated migmatite. The leucosomes separated for Sr and Nd isotopic analysis are 0.5–1 cm thick. The term “migmatite” is applied to finely laminated migmatites without removal of any leucosomes



biotite schist (MBS) under both water-present and water-absent conditions at 10 and 6 kb, respectively (Patiño-Douce and Harris 1998). It is interesting to find that group A leucosomes are of granitic composition and group B leucosomes of trondhjemite-like composition, which suggests that group B leucosomes may have formed from water-saturated or H<sub>2</sub>O-fluxed melting reactions at significantly lower temperatures than group A leucosomes.

Metapelites, leucosomes, and migmatites can be distinguished in their trace-element compositions as well. The leucosomes have the lowest Ni, Cr, Sc, V, Nb, Zn, and La concentrations, as compared to those in both the migmatites and metapelites (Table 1). The metapelites have higher Rb/Sr ratios ranging from 0.62 to 3.01, than those of the leucosomes (<0.50). Ba and Rb concentrations in the leucosomes are positively correlated with their K<sub>2</sub>O (wt%) contents (Fig. 5e and 5f). Nb and V concentrations are positively correlated with TiO<sub>2</sub> contents of leucosomes, migmatites, and metapelites (Fig. 6). The leucosomes have lower Nb (<13 ppm) and V (<64 ppm) concentrations than those of the migmatites and metapelites, which are greater than 15 ppm and 64 ppm, respectively. Trace-element data on the leucosomes fall into two groups: group A leucosomes have higher Rb, Ba, and Pb concentrations, and higher Rb/Sr ratios than those of group B (Fig. 5). All samples show LREE enrichment characteristics in a chondrite normalized REE diagram (Fig. 7). Except for one leuco-

some which has positive Eu anomalies, all the other samples show consistent negative Eu anomalies. We will return to these data following the presentation of the radiogenic isotopic data.

## Sr and Nd isotopic geochemistry

Radiogenic isotopic data for Sr and Nd are given for metapelites, migmatites, and leucosomes in Table 2. Figure 8 shows the isotopic compositions of samples analyzed on an  $\epsilon_{\text{Nd}}(T)$  versus  $^{87}\text{Sr}/^{86}\text{Sr}(T)$  diagram. A value of 100 Ma was assigned for  $T$  to evaluate the radiogenic isotopic composition at the time of migmatization (Zeng 2003; Saleeby and Zeng 2005). Rb and Sr concentrations in the leucosomes range from 12 ppm to 134 ppm, and 260 ppm to 675 ppm, respectively. Metapelites have Rb and Sr concentrations ranging from 88 ppm to 176 ppm, and 57 ppm to 247 ppm, respectively. Migmatites (including the proximal hosts for thickened leucosome samples) have Rb and Sr concentrations ranging from 91 ppm to 168 ppm, and 137 ppm to 471 ppm, respectively. Some of the proximal host samples have high Sr concentrations of up to 471 ppm. This may be due to concentration of Sr-rich minerals (e.g., feldspars) in the leucosome lamina. Compared with the metapelites, the leucosomes have low Rb/Sr ratios. Sm and Nd concentrations in the leucosomes range from 1.6 ppm to 6.3 ppm, and 10.2 ppm to 27.7 ppm, respectively. The metapelites have Sm and Nd concentrations ranging from 4.9 ppm to 9.5 ppm, and 26.5 ppm to 52.3 ppm, respectively. The migmatites have Sm and Nd concentrations ranging from 5.6 ppm to 8.4 ppm, and 21.1 ppm to 47.5 ppm, respectively. Based on their Rb concentrations, and Rb/Sr and Sm/Nd ratios, the leucosomes can be subdivided into group A and group B as well. Group A has high Rb concentrations (>100 ppm), Rb/Sr (0.15–0.5), and Sm/Nd (>0.20) ratios. In contrast, group B has low Rb concentrations (<20 ppm), low Rb/Sr (<0.10), and Sm/Nd (<0.20) ratios.

The leucosomes have a much wider range of  $\epsilon_{\text{Nd}}(T)$  values than the migmatites and metapelites, but they have a similar range of initial  $^{87}\text{Sr}/^{86}\text{Sr}$  ratios. The initial  $^{87}\text{Sr}/^{86}\text{Sr}$  ratios of leucosomes range from 0.7124 to 0.7247, similar to those of the metapelite protoliths (0.7125 to 0.7221). However, the leucosomes have initial  $\epsilon_{\text{Nd}}$  values ranging from –6.0 to –11.0, as compared to –8.7 to –11.3 for the metapelites, which implies that partial melting was in disequilibrium with respect to the Sm–Nd isotope system. As shown in Fig. 8, group A leucosomes have higher initial  $\epsilon_{\text{Nd}}$  values (>–7.0) and  $^{87}\text{Sr}/^{86}\text{Sr}$  ratios (>0.7145) than those of group B leucosomes.

In summary, two groups of leucosomes have been identified based on their trace element, Sr–Nd isotopic, and major element geochemical characteristics: (1) group A leucosomes, including samples L0406, L0407,

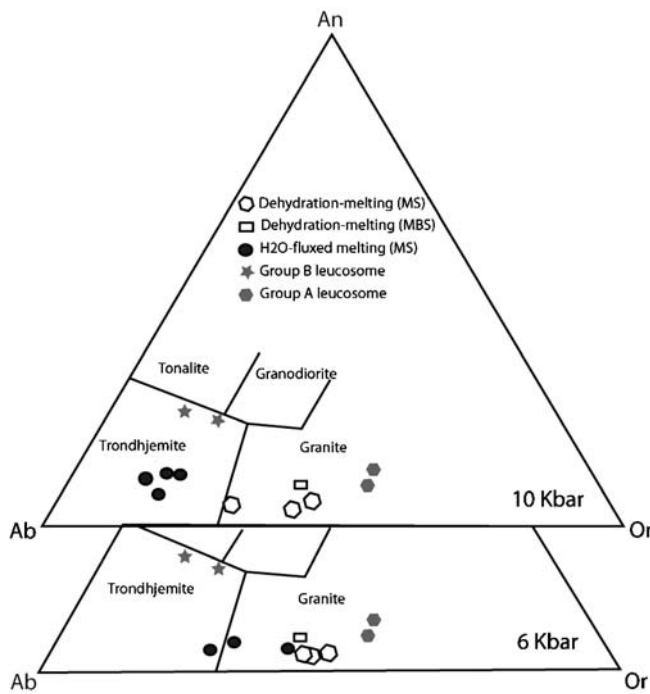


**Fig. 4** Normative albite (*Ab*)-anorthite (*An*)-orthoclase (*Or*) contents of the leucosomes compared with experimentally generated melt compositions (after Patiño-Douce and Harris 1998). Two leucosomes are plotted within the trondhjemite field, and the others in the granite field. The Ab–An–Or classification for silicic rocks was proposed by Barker (1979)

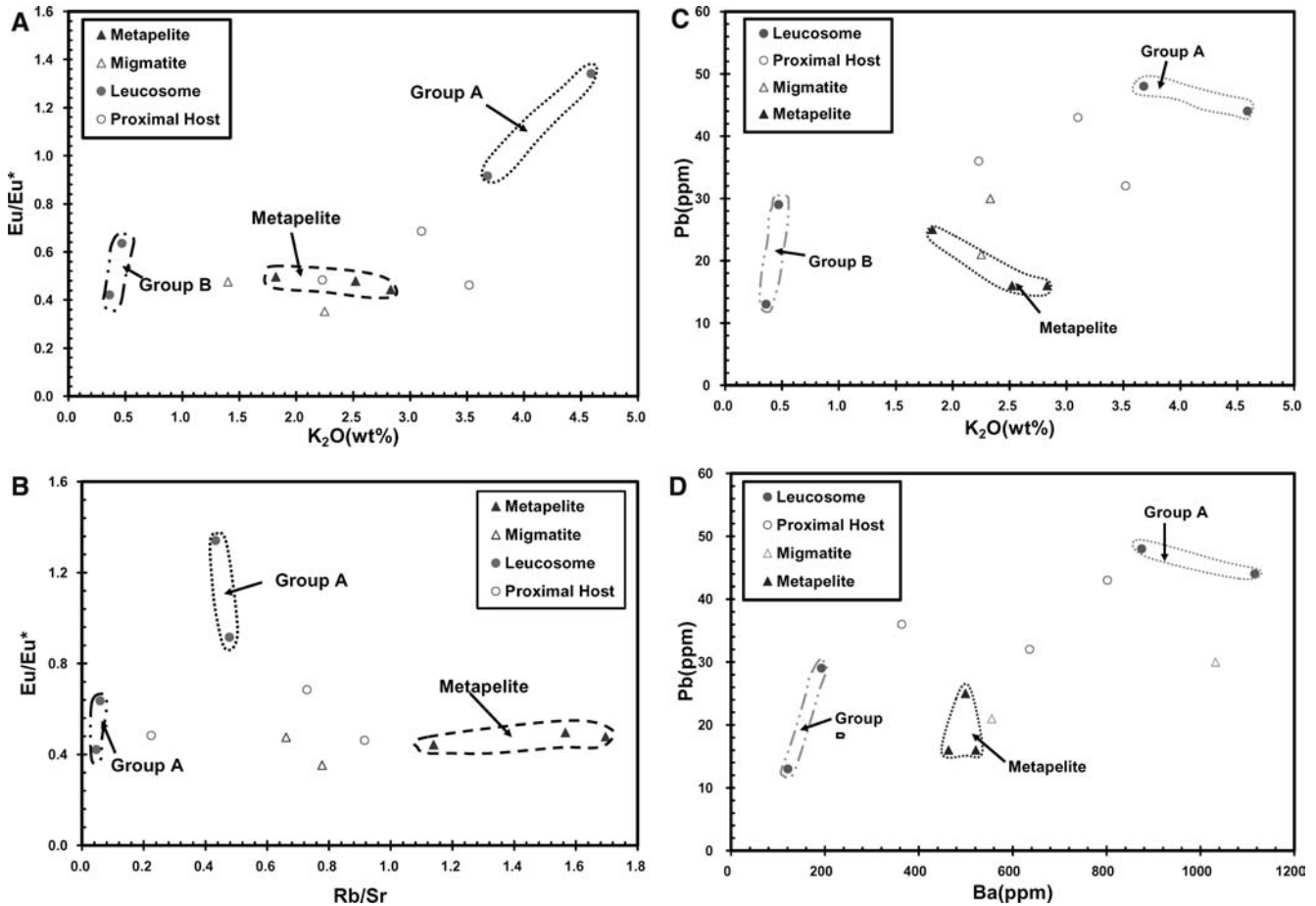


**Fig. 5** Covariation diagrams showing the relationships between **a** Eu anomaly and K<sub>2</sub>O (wt%), **b** Eu anomaly and Rb/Sr ratio, **c** Pb and K<sub>2</sub>O (wt%), **d** Pb and Ba, **e** Ba and K<sub>2</sub>O (wt%), and **f** Ba and Rb for the leucosomes, migmatites, and metapelites. These diagrams suggest that positive Eu anomalies of leucosomes arose from the increasing contribution of K-feldspar to the melt

and L0410, have higher initial  $\epsilon_{\text{Nd}}$  values ( $> -7.0$ ) than the migmatites and metapelite protoliths ( $< -8.5$ ), positive or slightly negative Eu anomalies, high Pb, Ba, Rb, and K<sub>2</sub>O contents, high  $^{87}\text{Sr}/^{86}\text{Sr}$  ratios ( $> 0.7145$ ), and are of granitic composition; and in contrast, (2) group B leucosomes including samples of L0404 and L0405, have similar initial  $\epsilon_{\text{Nd}}$  values to those of the migmatites and metapelites, significant negative Eu anomalies, low Pb, Ba, Rb, and K<sub>2</sub>O contents, low  $^{87}\text{Sr}/^{86}\text{Sr}$  ( $< 0.7145$ ) ratios, and are of trondhjemite-like composition. Finally, as shown in Fig. 10a, there is a relative enrichment of Sr in the migmatites (Fig. 10a) as compared to the metapelite protolith.

## Discussion

First, we will briefly discuss the possible melting reactions under the attendant  $P$ - $T$  conditions during the emplacement of the southern Sierra Nevada batholith at  $\sim 100$  Ma. In isotopic disequilibrium melting, the isoto-

pic composition of a given isotope in the melt depends on its concentrations and isotopic compositions in the minerals of the initial solid and on the mineral proportions which dissolve into the melt (Allègre and Minster 1978). Recent studies of migmatites (Barbero et al. 1995) and of pelitic gneisses and leucogranite in the Himalayas (George and Bertlett 1996) show that Sr and Nd isotopic heterogeneity can be preserved on the mineralogic scale before and during anatexis. Deniel et al. (1987) presented Sr and Nd isotopic composition data of the Manaslu granite, Himalayas, Nepal and demonstrated a wide range of initial Sr and Nd isotopic ratios and an isotopic heterogeneity on a meter scale in the source that has not been obliterated by magmatic processes. These results suggest that isotopic heterogeneity among phases in a source rock may be well preserved until a major melting event, which is consistent with the observations of fine-scale disequilibrium and extremely sluggish of metamorphic reactions on metamorphic rocks (Baxter and DePaolo 2000; Carlson 2002). Such field and experimental observations contradict theoretical considerations, which suggest that isotopic heterogeneity in the source may not survive prograde heating during collisional orogenesis (Harris and Ayres 1998). Rapid heating induced by external heat source such as shear heating on a major shear zone, input from magma underplating, or intrusion may favor isotopic disequilib-

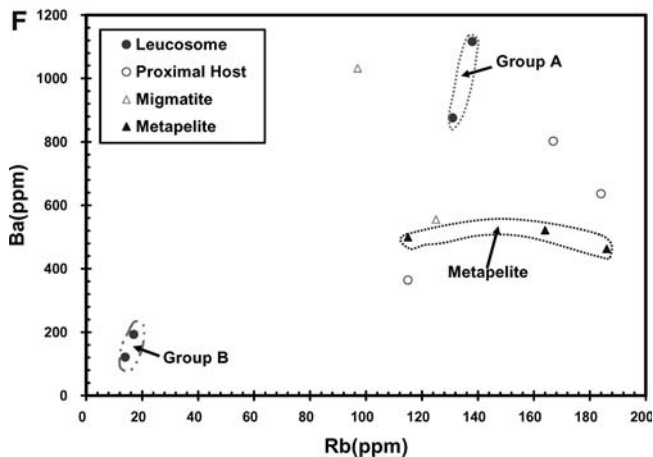
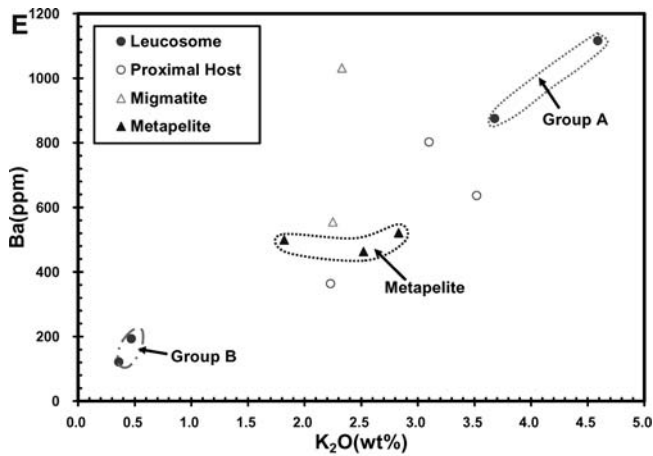


Fig. 5 (Contd.)

rium melting (Harrison et al. 1999; Petford and Gallagher 2001). The supracrustal rocks (e.g. the Kings Sequence metasedimentary framework rocks in the Sierra Nevada batholith) have experienced a protracted history of intrusion of granitic plutons since 200 Ma. It is very possible that a large amount of detrital mineral grains within the labile metasedimentary rocks have preserved different isotopic compositions as compared to other newly formed ones. Therefore, it is worth exploring Sr and Nd isotopic systematics of anatexitic melts by assuming nonhomogenous isotopic compositions between melting phases and examining whether such a model can account for the observed Sr–Nd isotopic systematics of the leucosomes with respect to the metapelites and migmatites.

#### Common melting reactions and their characteristics

Aluminous schists and gneisses are generally considered to be likely sources for peraluminous granitic melts (Wyllie 1977; Vielzeuf and Holloway 1988; Le Breton and Thompson 1988; Rushmer 1991; Vielzeuf and Montel 1994; Patiño-Douce and Beard 1995, 1996; Thompson 1996; Patiño-Douce and Harris 1998; Knesel

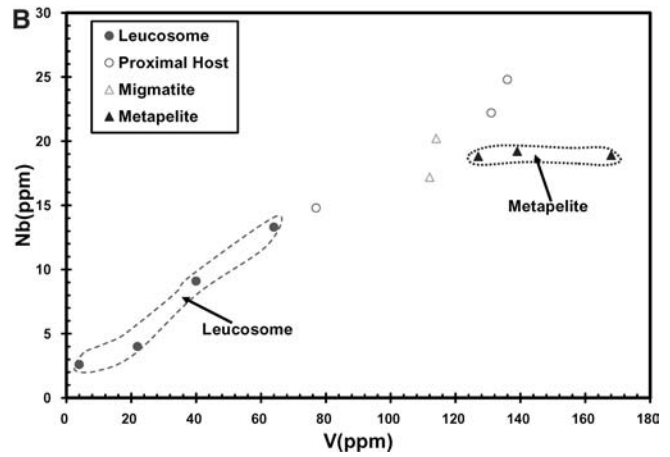
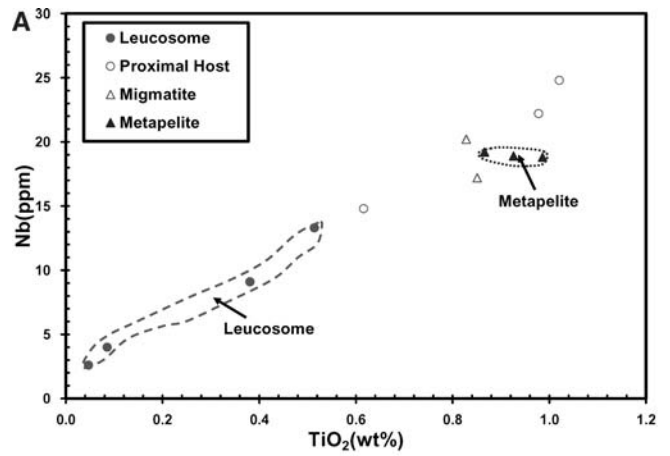
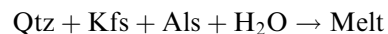


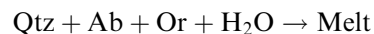
Fig. 6 Plots of **a** Nb versus  $\text{TiO}_2$  (wt%). **b** Nb over V. These plots show that both Nb and V in the leucosomes, migmatites, and metapelites are negatively correlated with the contents of Ti, suggesting that ilmenite stayed as a residue phase during the partial melting of the upper pelite protolith

and Davidson 2002; Whittington and Treloar 2002). For pelitic and quartzo-feldspathic rocks, the melting reactions that produce granitic melts are listed as following in the order of increasing melting temperatures (Fig. 9):

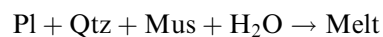
1. Water-saturated melting reaction



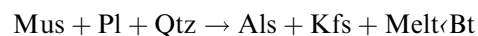
2. Water-saturated melting reaction



3.  $\text{H}_2\text{O}$ -fluxed melting of muscovite-bearing pelite



4. Fluid-absent muscovite dehydration melting



5. Fluid-absent biotite dehydration melting after exhaustion of muscovite

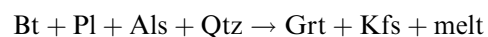


**Fig. 7** REE diagram showing the REE characteristics of the leucosomes, migmatites, and metapelites. REE are normalized to the primitive mantle (PM) (Sun and McDonough 1989). Except for two leucosomes which have positive or slightly negative Eu anomalies, the rest of the samples have consistently negative Eu anomalies. Leucosome: L0404, L0405, L0407, and L0410; Proximal host: R0404, R0407, and R0410; Finely laminated migmatite: Li9805 and Li9808; Metapelite: PP0101, PS0101, and Li9815

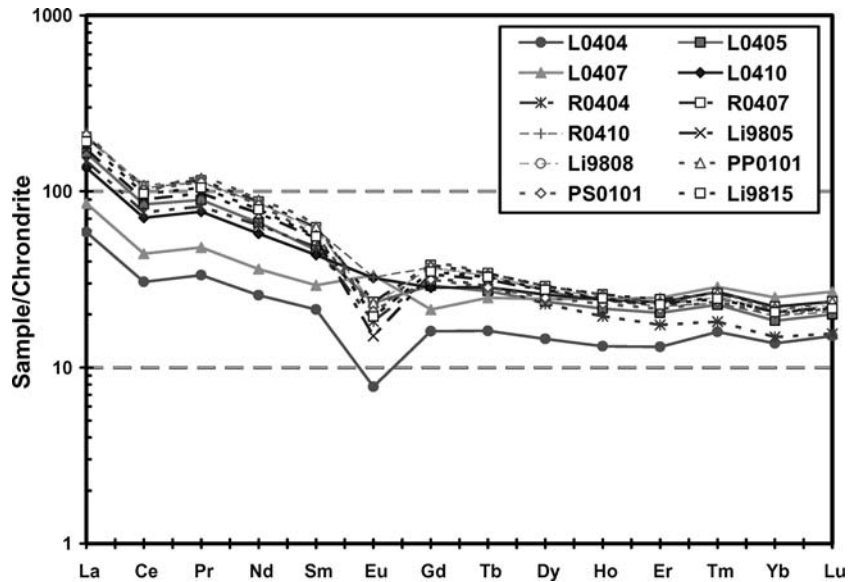
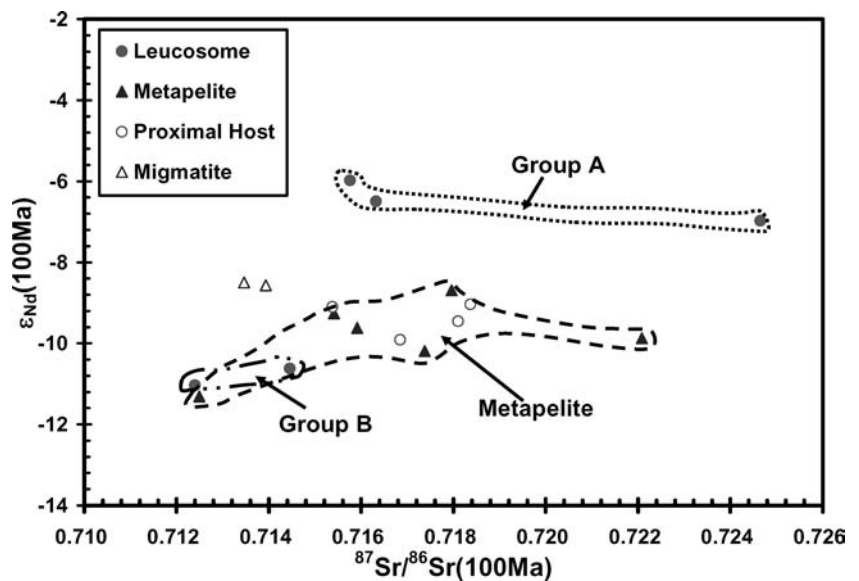


**Fig. 8** Nd–Sr radiogenic isotopic systematics of the metapelite protoliths, migmatites, and leucosomes. The diagram shows that the leucosomes have a much wider range of initial  $\epsilon_{Nd}$  values than the metapelite protoliths, but they have similar ranges of initial Sr isotopic ratios, suggesting that melts that formed the group A leucosomes are in Nd isotopic disequilibrium with respect to their protoliths



where Qtz, Ab, Or, Kfs, Als, Pl, Mus, Bt, and Grt are quartz, albite, orthoclase, K-feldspar, aluminosilicate, plagioclase, muscovite, biotite, and garnet, respectively (after Kretz 1983). For these melting reactions, muscovite dehydration melting reactions occur at much lower temperatures ( $< 750$  °C) as contrasted with  $\sim 825$  to  $900$  °C for biotite dehydration melting, and result in a lower degree of partial melting due to higher water contents of melts buffered by the muscovite dehydration melting (Le Breton and Thompson 1988). Under the same  $P$ – $T$  conditions and for the same protolith, the influx of water has interesting effects on melting behavior. In partial melting without free water, water is liberated by breakdown of hydrous minerals such as muscovite and biotite. Such a melting reaction is referred to as dehydration partial melting. Water-saturated and water-fluxed partial melting reactions are

melting processes with excess water; both are water saturated. Water and fluid are used interchangeably in the following discussion. Increasing water activity depresses the feldspar + quartz solidus more strongly than it depresses the stability of micas, which limits the participation of muscovite. However, the onset of fluid-present melting will result in a reduced water activity in the protoliths as soon as water disappears or water content of mixed fluid diminishes, and thus drive the melting toward reactions with increasing proportions of hydrous minerals as in reaction 3, 4, and 5 at higher temperatures, except in the geologically improbable case of a huge water reservoir accessible continuously to the protolith during melting. These interesting but complex features of crustal anatexis lead to the complicated melt products and geochemistry commonly observed in migmatite zones. Modeling of complex melting reactions in

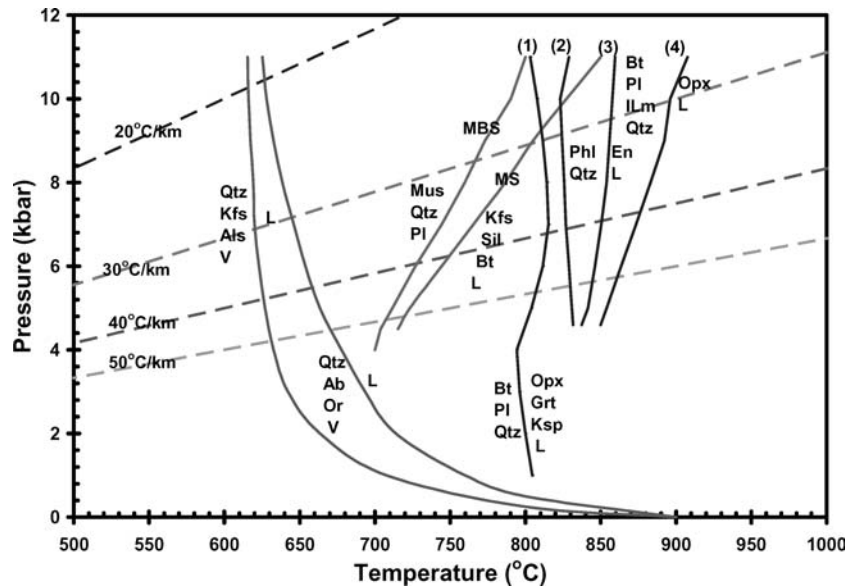


**Fig. 9**  $P$ - $T$  diagram showing experimentally determined solidus and melting reactions for a metasedimentary source (after Whittington and Treloar 2002). Water-saturated melting reaction  $Qtz + Ab + Or + H_2O = M$  from Ebadi and Johannes (1991). Calculated locus of water-saturated melting reaction  $Qtz + Kfs + Als + H_2O = M$  from Johannes and Holtz (1996). Dehydration melting reactions  $Qtz + Ms + Pl = Kfs + Sil + Bt + M$  (natural system) for muscovite-biotite schist (*MBS*) and muscovite schist (*MS*) from Patiño-Douce and Harris (1998). Biotite dehydration melting reaction (1)  $Bt + Pl + Qtz = Opx + Grt + Kfs + M$  (natural system) from Vielzeuf and Montel (1994), (2) and (4)  $Bt + Pl + Qtz = Opx + M$  (natural system) from Patiño-Douce and Beard (1995), and (3)  $Phl + Qtz = En + M$  (MASH system) from Vielzeuf and Clemens (1992). Typical geothermal gradients for the continental crust are also shown in this diagram. *M* melt, *Qtz* Quartz, *Ab* albite, *Or* orthoclase, *Kfs* K-feldspar, *Als* aluminosilicate, *Ms* muscovite, *Pl* plagioclase, *Sil* sillimanite, *Bt* biotite, *Opx* orthopyroxene, *Grt* garnet, *Phl* phlogopite, *En* enstatite, *Ilm* ilmenite, *Cpx* clinopyroxene, *L* melt, *V* vapor or water. Mineral abbreviations are after Kretz (1983)

pelitic protoliths, and the geochemical consequences of dehydration melting of muscovite and biotite in metapelites, has been explored by Harris and Inger (1992), Inger and Harris (1993), and Harris et al. (1995). They showed that three melting reactions (reaction 3, 4, and 5) that involve hydrous minerals in different roles have distinctive restite mineralogies that controls the trace-element distribution between the sources and melts. Depending on the  $P$ - $T$  conditions, water activity ( $\alpha_{H_2O}$ ), and protolith mineral assemblages, these reactions would control both the volume of melt produced and the mineralogy of the restites. These reactions in turn control the trace-element and radiogenic isotopic compositions of the resultant melt. The variations in radiogenic isotopic compositions of the melts result from different isotopic compositions in the various phases that undergo partial melting, if each reactant phase could preserve its radiogenic isotopic composition until the onset of melting. In terms of the mass proportions of muscovite relative to plagioclase entering the

melts, reaction 3 has a muscovite/plagioclase ratio of 0.6, which is significantly less than the value of 3.1 for reaction 4 (Patiño-Douce and Harris 1998). Taking the Rb-Sr system as an example, because muscovite and biotite are the principal hosts of Rb, and plagioclase and K-feldspar for Sr, the differences in muscovite/plagioclase ratios between reaction 3 and 4 result in distinctive Rb/Sr ratios and Sr isotopic compositions of the melts produced by reaction 3 from those by reaction 4, assuming micas have different Sr isotopic compositions from those in feldspars. Note that under water-saturated conditions, partial melting is dominated by melting of quartz + feldspar (reaction 1 and 2) and muscovite or biotite is largely excluded from such partial melting reactions even though there are abundant micas in a pelitic source. Consequently, isotopic disequilibrium melting of reaction 1 and 2 results in melts having low Rb/Sr and  $^{87}Sr/^{86}Sr$  ratios. For the temperature range under consideration, one of the reactions (reaction 1 through 4) predominates in the melt production. Moreover, these partial melting processes not only modify the orthoclase/albite ratio by varying proportions of plagioclase entering the melt and by K-feldspar forming as a residual phase, they also influence the contents of Ba, Na, and Pb, as well as the ratios of Rb/Sr,  $K_2O/Na_2O$ , and Sm/Nd in the melt by varying proportions of muscovite and biotite with respect to plagioclase and K-feldspar consumed during partial melting (Inger and Harris 1993; Guillot 1993). Based on the petrographic and geochemical data, the potential major phases that were involved in the partial melting of the Isabella pendant upper pelite unit are muscovite, biotite, K-feldspar, quartz, plagioclase, and aluminosilicate (principally andalusite). Muscovite, biotite, and feldspars are the dominant phases that would regulate the partitioning of Rb, Sr, Ba, Pb, and K between the melt and residue. Therefore, these element concentrations of the leucosomes would be good indices for the

melting processes during the formation of migmatite in this area.

### Melting of muscovite

Below, we interpret the trace-element and isotopic data for the leucosomes and migmatites in the context of melting of muscovite. In contrast to Sr, Rb is more compatible with biotite than muscovite and feldspar (Peucat 1986; Henderson 1982; Nash and Crecraft 1985) such that: (1) biotite is characterized by the highest Rb/Sr ratio and relatively high-time integrated  $^{87}\text{Sr}/^{86}\text{Sr}$  ratio due to radioactive decay of  $^{87}\text{Rb}$ ; (2) muscovite has the intermediate Rb/Sr and  $^{87}\text{Sr}/^{86}\text{Sr}$  ratios; and (3) feldspar (plagioclase and K-feldspar) has the lowest Rb/Sr and  $^{87}\text{Sr}/^{86}\text{Sr}$  ratios, as compared to the bulk-rock values. The  $P$ - $T$  conditions of migmatization that were outlined above indicate temperatures below that of biotite dehydration partial melting, which occurs generally in the range of 825–900 °C under fluid-absent conditions (Clemens and Vielzeuf 1987; Patiño-Douce and Johnston 1991). High modal contents of biotite, which is typically in excess of 60% in the melanosomes of the migmatites, also suggest that biotite was not involved significantly in partial melt production, or biotite formed as a product of muscovite dehydration melting of reaction 4. However, this would give rise to very low Rb concentrations and relatively unradiogenic Sr isotopic compositions in the leucosomes as compared to their sources, which is not evident in the data. The rarity of garnet coexisting with biotite and K-feldspar, even at localities of highest temperatures in the proximity of the Goat Ranch pluton, also suggests that fluid-absent biotite dehydration melting did not play a significant role in generating the migmatite zone. Based on the trace element and Rb-Sr isotopic data of the leucosomes, we suggest that most of the leucosomes were derived from partial melting of quartz + K-feldspar + plagioclase assemblages with or without involvement of muscovite under fluid-present conditions. An important feature shown in the Rb-Sr isotopic systematics (Fig. 10b) of the leucosomes is that their initial  $^{87}\text{Sr}/^{86}\text{Sr}$  ratios are positively correlated to their Rb/Sr ratios. This relation indicates that those leucosomes with relatively elevated Rb/Sr ratios resulted from increasing proportions of muscovite over feldspar entering the melt. The control of initial  $^{87}\text{Sr}/^{86}\text{Sr}$  of anatectic melts by the relative proportions of muscovite over feldspar entering the melt has been observed experimentally by Knesel and Davidson (2002) and evaluated theoretically by Zeng et al. (2005b). One leucosome sample from the study area (L0410) stands out from the rest by its highest Rb/Sr and initial  $^{87}\text{Sr}/^{86}\text{Sr}$  ratios (Fig. 10b). We suggest that this marks fluid-absent muscovite dehydration melting in the production of that particular leucosome layer. Group A leucosomes have high Rb concentrations that overlap with those in the metapelites, and higher Rb/Sr ratios than group B leucosomes, which suggests a greater

proportion of muscovite entering the group A melts. Group B leucosomes have lower Rb concentrations than the metapelites by about an order of magnitude. This is evidence against these leucosomes being generated from either fluid-absent muscovite or biotite dehydration melting, since both melting reactions generally result in melts with Rb/Sr ratios greater than 1.0. Group A leucosomes might be derived either from fluid-absent muscovite dehydration melting with biotite in the restite, or from  $\text{H}_2\text{O}$ -fluxed melting of muscovite. Group B leucosomes may in contrast be derived from  $\text{H}_2\text{O}$ -fluxed melting of muscovite or water-saturated melting of quartz and feldspar assemblage. This interpretation is consistent with the inferences drawn based on the major element compositions of the leucosomes (Fig. 4).

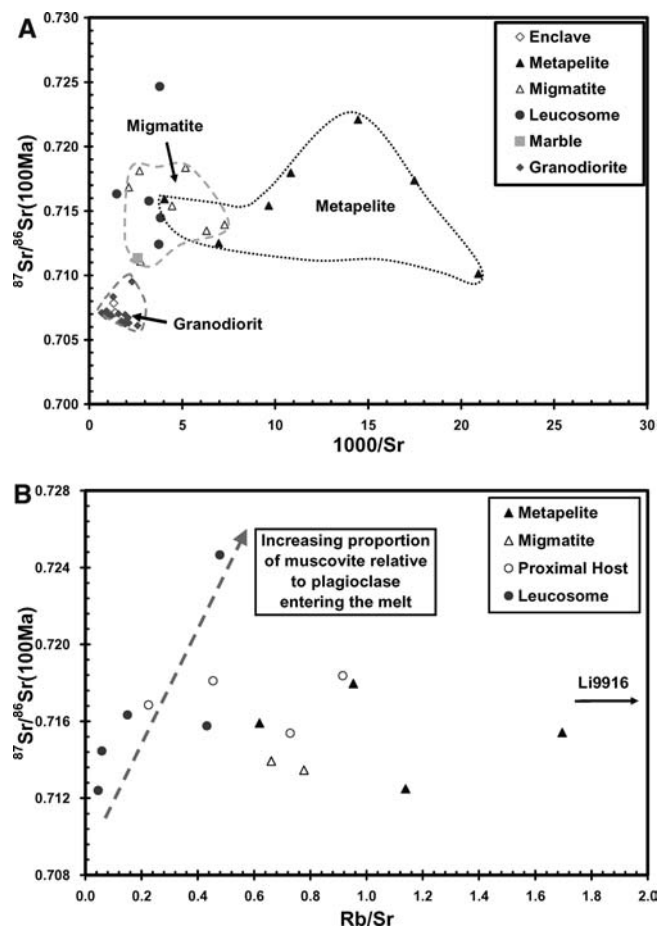


**Fig. 10** a Sr isotopic compositions of the metapelites, migmatites (proximal host and finely laminated migmatite), and leucosomes showing the higher Sr concentrations in the leucosomes than those in the pelite protoliths. For comparison, it also shows the Sr isotopic compositions of the Goat Ranch granodiorite and enclave samples. The Goat Ranch data are from Zeng (2003). b The initial  $^{87}\text{Sr}/^{86}\text{Sr}$  ratios of the metapelites, migmatites, and leucosomes are plotted against their respective Rb/Sr ratios. It shows that initial  $^{87}\text{Sr}/^{86}\text{Sr}$  ratios of the leucosomes roughly increase with their Rb/Sr ratios, suggesting an increasing proportion of muscovite relative to plagioclase entering the melt

## K-feldspar signature

The significant role of K-feldspar in the partial melting of metapelites was reported to have given rise to positive Eu anomalies of leucosomes (Harris et al. 1986; McDermott et al. 1996). Figure 5a shows that positive or weak negative Eu anomalies of group A leucosomes are associated with their high  $K_2O$  contents. For crustal rocks, K-feldspar is the major phase that hosts Pb. The positive correlation between Pb and  $K_2O$  in the group A leucosomes, migmatites, and metapelite protoliths (Fig. 5c) also suggests that positive or weak negative Eu anomalies of group A leucosomes arise from either the melting or entrainment of K-feldspars. Alkali feldspars commonly have Ba concentrations ranging from 1,000 ppm to 10,000 ppm, significantly higher than those of plagioclases. Fluid-absent conditions favor residual K-feldspar due to limited melt fraction, but at higher temperatures or increasing water activities, K-feldspar will melt in greater proportions (McDermott et al. 1996). This is marked by a decrease in the Rb/Sr ratio and increase in Ba content of a melt, which also characterizes the trace-element geochemistry of the group A leucosomes (Fig. 5e). The Ba concentrations of group A leucosomes are higher than those of both migmatites and metapelites by a factor of three (Table 1).

Group A leucosomes may have been derived from muscovite dehydration melting reaction in which K-feldspar was also assimilated into the melt. Such assimilation would produce melts having low Rb/Sr ratios, positive or weak negative Eu anomalies, and elevated Sr, Ba, Pb, and K contents. In contrast, group B leucosomes might represent the melting products from K-feldspar-limiting  $H_2O$ -fluxed muscovite melting or melting of quartz + feldspar assemblages, which results in melts having low Rb/Sr ratio, negative Eu anomalies, and decreased Pb, Ba, and K concentrations (Fig. 5).

## The role of accessory phases

Previous studies have shown that accessory minerals such as zircon, apatite, ilmenite, and monazite play a critical role in controlling the distribution of trace elements such as Zr, Hf, Sm, Nd, U, Th, Nb, and Pb between melt products and residues (Rapp and Watson 1986; Hogan and Sinha 1991; Bea et al. 1994; Ayres and Harris 1997; Zeng et al. 2005a, b). Ilmenite is the predominant host for Ti as well as a variety of trace elements such as Nb, Ta, and V in metasedimentary rocks. Therefore, if ilmenite stayed as a residue during partial melting, the resultant leucosomes should have lower concentrations of Ti, Nb, Ta, and V than the residue as well as the protolith. Figure 6 shows that: (1) both Nb and V concentrations in the leucosomes, migmatites, and metapelites are positively correlated with their  $TiO_2$  (wt%) contents; (2) the leucosomes have lower concentrations of Nb (< 13 ppm) and V (< 64 ppm), and  $TiO_2$  contents than those in the metapelites and migmatites.

This suggests that ilmenite behaved as a residual phase during partial melting, and is consistent with the relatively high concentration of opaque minerals observed in melanosome lamina.

Geochemical observations and theoretical modeling have shown that dissolution of apatite may play an important role in shaping the Nd isotopic systematics of anatectic melts (Ayres and Harris 1997; Zeng et al. 2005b). The observation that elevated  $\epsilon_{Nd}(T)$  values of the leucosomes correspond to elevated  $P_2O_5$  contents suggests that the Nd isotopic compositions of the leucosomes may be strongly affected by the dissolution of apatite (Fig. 11). Group A leucosomes have substantially higher  $\epsilon_{Nd}(T)$  values and  $P_2O_5$  contents than those of group B, reflecting a greater apatite component and possibly higher temperature of melting. Increased

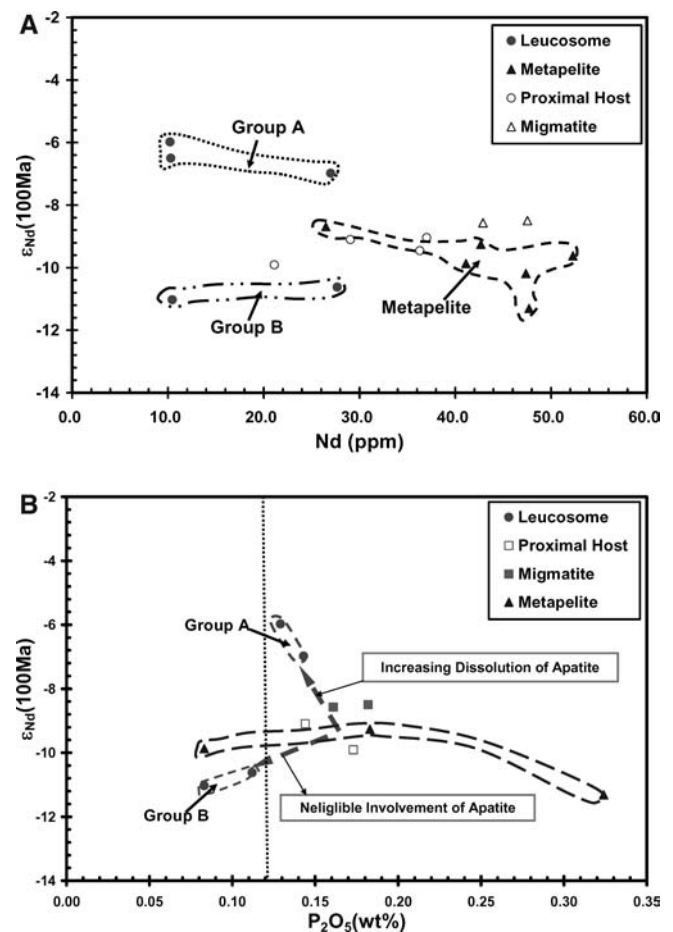


**Fig. 11** a Nd isotopic compositions of the metapelites, migmatites, and leucosomes plotted against Nd concentrations. Melts from the pelitic source have lower Nd concentrations and wider initial  $\epsilon_{Nd}$  values than their sources. b Plot of the initial  $\epsilon_{Nd}$  values of the metapelites, migmatites, and leucosomes versus their respective  $P_2O_5$  content (wt%). Group A leucosomes have higher initial  $\epsilon_{Nd}$  values than their sources. In contrast, group B leucosomes have similar initial  $\epsilon_{Nd}$  values to their sources. The correlation of the initial  $\epsilon_{Nd}$  values of the leucosomes with their  $P_2O_5$  content (wt%) suggests that those high initial  $\epsilon_{Nd}$  values may be due to increasing dissolution of apatite during melting

dissolution of apatite into melt requires higher temperature conditions because water has little effect in the dissolution of apatite (Harrison and Watson 1984). The inference of higher temperature conditions for the formation of group A leucosomes is in accordance with the conclusion drawn based on the correlations among K<sub>2</sub>O, Pb, and Ba contents, and positive or weak negative Eu anomalies as discussed in the previous section. The dissolution behavior of apatite may also strongly influence the Nd isotopic systematics of melt products (Zeng et al. 2005b). For example, contrasted to monazite, apatite usually has a higher Sm/Nd ratio and thus high time-integrated  $\epsilon_{Nd}$  values relative to those of the bulk rock (Ayres and Harris 1997). Dissolution or entrainment of apatite into the melt will elevate both the Sm/Nd ratio and  $\epsilon_{Nd}$  value of the melt. The large variations in Sm/Nd ratios of the leucosomes from 0.11 to 0.33, and elevated  $\epsilon_{Nd}(T)$  values as compared to their sources suggest the important role of accessory minerals in fractionation Sm from Nd and developing Nd isotopic disequilibrium during crustal anatexis (Zeng et al. 2005a).

---

## Conclusions

We have performed major and trace element and radiogenic isotopic studies on a suite of leucosomes, their complementary proximal hosts, migmatites, and metapelites. We found that the leucosomes fall into two groups: (1) group A leucosomes have higher initial  $\epsilon_{Nd}$  values ( $> -7.0$ ) than the migmatites and metapelites ( $< -8.5$ ), positive or weak negative Eu anomalies, high Pb, Ba, Rb, and K<sub>2</sub>O contents, high  $^{87}Sr/^{86}Sr$  ratios ( $> 0.7145$ ), and are of granitic composition; and in contrast, (2) group B leucosomes have similar initial  $\epsilon_{Nd}$  values to those of the migmatites and metapelites, negative Eu anomalies, low Pb, Ba, Rb, and K<sub>2</sub>O contents, low  $^{87}Sr/^{86}Sr$  ratios ( $< 0.7145$ ), and are of trondhjemitic-like composition. These data can be modeled as a result of nonmodal partial melting of the pelite protolith. Given the relatively low temperatures of the metamorphic reactions at the level of exposure and observation, and low contents of muscovite and plagioclase and high contents of K-feldspar in the pelitic protolith, group B leucosomes may represent melts from fluid-present partial melting reactions of quartz + feldspar assemblages (reaction 1 and 2). Intensive concurrent hydrothermal activity as evidenced by skarn deposits in the stratigraphically adjacent marble unit as well as pegmatitic dikes may have limited the role of fluid-absent muscovite dehydration melting in the production of leucosomes, even though the major and trace element and radiogenic isotopic data suggest that some of group A leucosomes may have formed from such a reaction.

In summary, we show that during the formation of the migmatite zone in the Isabella pendant: (1) the leucosomes were partial melting products; (2) trace element and radiogenic isotope geochemistry data suggest that crustal anatexis could generate a spectrum of

leucogranitic melts with various major, trace element, and radiogenic isotopic compositions; (3) Sm and Nd isotopic compositions of the leucosomes suggest the disequilibrium nature of nonmodal crustal anatexis and small degrees of parent/daughter fractionation by accessory phases during partial melting; (4) both leucosomes and metapelites have a high degree of isotopic heterogeneity; and (5) trace minerals such as ilmenite play a dominant role in controlling the redistribution of key trace elements such as Nb, V, and Ta between the melt products and solid residue. The data presented here also suggest that: (1) the behavior of the Rb–Sr system is controlled by the melting behavior of feldspars versus micas, which are in turn controlled by H<sub>2</sub>O fugacity; and (2) the behavior of the Sm–Nd system is largely controlled by accessory phases (e.g., apatite) as long as garnet is not a major phase during partial melting of metasedimentary rocks.

Field, geochemical, and isotopic data from this study suggest that formation of a migmatite zone within the pre-existing metaclastic country rocks in response to thermal perturbations induced by the impingement of hot silicic magma is a potentially important mechanism to help differentiate the continental crust into more silicic upper crust and corresponding mafic parts. If melts generated by crustal anatexis can segregate and migrate to shallower levels of the crust, heat-producing (U, Th, and K), LILE, and LREE elements can be efficiently redistributed into the shallow crust. The various degrees of parent/daughter fractionation of both the Rb–Sr and Sm–Nd systems as a consequence of crustal anatexis would render distinct isotopic reservoirs that could profoundly influence the products of subsequent mixing events. This is not only critical for intracrustal differentiation, but also potentially an important process in generating crustal isotopic heterogeneities. Because some of granitic batholiths acquire their crustal signatures by wallrock-derived melt contamination, complicated Sr and Nd isotopic compositions of crustally derived melts require extreme care in interpreting batholithic Sr and Nd systematics.

**Acknowledgements** Support for this research was provided by NSF grants EAR-9815024 and EAR-0087347. We thank H.P. Taylor, P. Asimow, J. Eiler, and G. Rossman for critical comments on an early version of this manuscript. We thank A.E. Patiño-Douce and C. Miller who gave thoughtful and constructive reviews and I. Carmichael for handling this manuscript.

---

## References

- Ague JJ (1997) Thermodynamic calculation of emplacement pressures for batholithic rocks, California: implications for the aluminum-in-hornblende barometer. *Geology* 25:563–566
- Ague JJ, Brimhall GH (1987) Granites of the batholiths of California: products of local assimilation and regional-scale crustal contamination. *Geology* 15:63–66
- Allègre CJ, Minster JF (1978) Quantitative models of trace element behavior in magmatic processes. *Earth Planet Sci Lett* 38:1–25

- Ayres M, Harris N (1997) REE fractionation and Nd-isotope disequilibrium during crustal anatexis: constraints from Himalayan leucogranites. *Chem Geol* 139:249–269
- Barbero L, Villaseca C, Rogers G, Brown PE (1995) Geochemical and isotopic disequilibrium in crustal melting: an insight from the anatectic granitoids from Toledo, Spain. *J Geophys Res* 100:15745–15765
- Baxter EF, DePaolo DJ (2000) Field measurement of slow metamorphic reaction rates at temperatures of 500° to 600°C. *Science* 288:1411–1414
- Bea F (1996a) Controls on the trace element composition of crustal melts. *Trans R Soc Edinburg Earth Sci* 87:133–141
- Bea F (1996b) Residence of REE, Y, Th and U in granites and crustal protoliths: implications for the chemistry of crustal melts. *J Petrol* 37:521–552
- Bea F, Montero P (1999) Behaviour of accessory phases and redistribution of Zr, REE, Y, Th, and U during metamorphism and partial melting of metapelites in the lower crust: an example from the Kinzigite formation of Ivrea-Verbano, NW Italy. *Geochim Cosmochim Acta* 63:1133–1153
- Bea F, Pereira MD, Stroh A (1994) Mineral/leucosome trace-element partitioning in a peraluminous migmatite (a laser ablation-ICP-MS study). *Chem Geol* 117:291–312
- Best MG, Weiss LE (1964) Mineralogical relations in some pelitic hornfels from the southern Sierra Nevada, California. *Am Miner* 49:1240–1266
- Carlson WD (2002) Scales of disequilibrium and rates of equilibration during metamorphism. *Am Miner* 87:185–204
- Clemens JD, Vielzeuf D (1987) Constraints on melting and magma production in the crust. *Earth Planet Sci Lett* 86:287–306
- Dardien V, Thompson AB, Grujic D, Ulmer P (1995) Experiment melting of biotite + plagioclase + quartz ± muscovite assemblages and implications for crustal melting. *J Geophys Res* 100:15581–15591
- Deniel C, Vidal P, Fernandez A, Le Fort P, Peucat JJ (1987) Isotopic study of the Manaslu granite (Himalaya, Nepal): inferences on the age and source of the Himalayan leucogranites. *Contrib Miner Petrol* 96:78–92
- Dixon ET (1995) An evaluation of hornblende barometry, Isabella to Tehachapi region, southern Sierra Nevada, California: The University of Michigan, MS Thesis, p 178
- Ducea MN, Saleeby JB (1998) The age and origin of a thick mafic-ultramafic keel from beneath the Sierra Nevada Batholith. *Contrib Miner Petrol* 113:169–185
- Ebadi A, Johannes W (1991) Beginning of melting and composition of first melts in the system Qz–Ab–Or–H<sub>2</sub>O–CO. *Contrib Miner Petrol* 106:286–295
- Elan R (1985) High grade contact metamorphism at the Lake Isabella North Shore roof pendant, Southern Sierra Nevada, California. PhD Thesis, University of Southern California, p 202
- Fyfe WS (1973) The granulite facies, partial melting and the Achaean crust. *Philos Trans R Soc Lond Ser A273*:457–461
- George MT, Bertlett JM (1996) Rejuvenation of Rb-Sr mica ages during shearing on the northwestern margin of the Nanga Parbat–Haramosh massif. *Tectonophysics* 260:167–185
- Harris N, Ayres M (1998) The implications of Sr-isotope disequilibrium for rates of prograde metamorphism and melt extraction in anatectic terrains. In: Treloar PJ, O'Brien PJ (eds) What drives metamorphism and metamorphic relations? *Geol Soc Am Spec Pub* 138:171–182
- Harris NBW, Inger S (1992) Trace element modeling of pelite-derived granites. *Contrib Miner Petrol* 110:46–56
- Harris N, Massey J (1994) Decompression and anatexis of Himalayan metapelites. *Tectonics* 13:1537–1546
- Harris NBW, Pearce JA, Tindle AG (1986) Geochemical characteristics of collision-zone magmatism. In: Coward, MP, Ries AC (eds) *Collision Tectonics*. *Geol Soc London Spec Publ* 19:67–81
- Harris N, Inger S, Massey J (1993) The role of fluids in the formation of the High Himalayan leucogranites. In: Treloar PJ, Searle MP (eds) *Himalayan Tectonics*: London, *Geol Soc Spec Publ* 74:391–400
- Harris NBW, Ayres M, Massey J (1995) Geochemistry of granitic melts produced during the incongruent melting of Muscovite: implications for the extraction of Himalayan Leucogranitic Magmas. *J Geophys Res* 100:15767–15777
- Harrison TM, Watson EB (1984) The behavior of apatite during crustal anatexis: equilibrium and kinetic considerations. *Geochim Cosmochim Acta* 48:1467–1478
- Harrison TM, Grove M, Kevin D, McKeegan KD, Coath CD, Lovera OM, Le Fort P (1999) Origin and episodic emplacement of the Manaslu Intrusive Complex, Central Himalaya. *J Petrol* 40:3–19
- Henderson P (1982) *Inorganic geochemistry*. Pergamon, Oxford, p 345
- Hogan JP, Sinha AK (1991) The effect of accessory minerals on the distribution of lead isotopes during crustal anatexis: a model. *Geochim Cosmochim Acta* 55:335–348
- Inger S, Harris N (1993) Geochemical constraints on leucogranite magmatism in the Langtang Valley, Nepal Himalaya. *J Petrol* 34:345–368
- Johannes W (1988) What controls partial melting in migmatite? *J Meta Geol* 6:451–465
- Johannes W, Holtz F (1996) *Petrogenesis and experimental petrology of Granitic rocks*. Springer, Heidelberg, Berlin, New York
- Johnson DM, Hooper PR, Conrey RM (1999) XRF analysis of rocks and minerals for major and trace elements on a single low dilution Li-tetraborate fused bead. *Adv X-ray Anal* 41:843–867
- Knesel KM, Davidson JP (2002) Insight into collisional magmatism from isotopic fingerprints of melting reactions. *Science* 296:2206–2208
- Kretz R (1983) Symbols for rock-forming minerals. *Am Miner* 68:277–279
- Le Breton N, Thompson AB (1988) Fluid-absent (dehydration) melting of biotite in metapelite in the early stages of crustal anatexis. *Contrib Miner Petrol* 99:226–237
- McDermott F, Harris NB, Hawkesworth CJ (1996) Geochemical constraints on crustal anatexis: a case study from the Pan-African Damara granitoids of Namibia. *Contrib Miner Petrol* 123:406–423
- Miller CF, Watson EB, Harrison TM, Brown PE (1988) Perspectives on the source, segregation and transport of granitoid magmas. *Trans Royal Soc Edinburgh Earth Sci* 79:135–156
- Nash WP, Crecraft HR (1985) Partition coefficients for trace elements in silicic magmas. *Geochim Cosmochim Acta* 49:2309–2322
- Patiño-Douce AE, Beard JS (1995) Dehydration-melting of biotite gneiss and quartz amphibolite from 3 to 15 kbar. *J Petrol* 36:707–738
- Patiño-Douce AE, Beard JS (1996) Effects of P, f(O<sub>2</sub>) and Mg/Fe ratio on dehydration-melting of model metagreywakes. *J Petrol* 37:999–1024
- Patiño-Douce AE, Harris N (1998) Experimental constraints on Himalayan Anatexis. *J Petrol* 39:689–710
- Patiño-Douce AE, Johnston AD (1991) Phase equilibria and melt productivity in the pelitic system: Implications for the origin of peraluminous granitoids and aluminous granulites. *Contrib Miner Petrol* 107:202–218
- Petford N, Gallagher K (2001) Partial melting of mafic (amphibolitic) lower crust by periodic influx of basaltic magma. *Earth Planet Sci Lett* 193:483–499
- Peucat JJ (1986) Behaviour of Rb–Sr whole rock and U–Pb zircon system during partial melting as shown in migmatitic gneisses from the St Malo Massif, NE Brittany, France. *J Geol Soc Lond* 143:875–885
- Pickett DA, Saleeby JB (1993) Thermobarometry of Cretaceous rocks of the Tehachapi Mountains, California: plutonism and metamorphism in deep levels of the Sierra Nevada batholith. *J Geophys Res* 98:609–629
- Pickett DA, Saleeby JB (1994) Nd, Sr and Pb isotopic characteristics of Cretaceous intrusive rocks from deep levels of the Sierra Nevada batholith, Tehachapi Mountains, California. *Contrib Miner Petrol* 118:198–215

- Rapp RP, Watson EB (1986) Monazite solubility and dissolution kinetics: implications for the Th and light rare-earth chemistry of felsic magmas. *Contrib Miner Petrol* 94:304–316
- Saleeby JB (1990) Progress in tectonic and petrogenetic studies in an exposed cross-section of young (~100 Ma) continental crust, southern Sierra Nevada, California. In: Salisbury MH (ed) *Exposed cross-section of the continental Crust*. NATO Advanced Studies Institute, pp 137–158
- Saleeby JB, Busby C (1993) Paleogeographic and tectonic setting of axial and western metamorphic framework rocks of the southern Sierra Nevada, California. In: Dunn G, MacDougall K (eds) *Mesozoic Paleogeography of Western United States-II*, Pacific Section SEPM, Book 71, pp 197–226
- Saleeby JB, Zeng L (2005) Structure and geochronology of plutonic and high-grade metamorphic rocks of the Lake Isabella area, southern Sierra Nevada, CA (in preparation)
- Sawyer EW (1998) Formation and evolution of granite magmas during crustal reworking: the significance of diatexites. *J Petrol* 39:1147–1167
- Sun S-S, McDonough WF (1989) Chemical and isotopic systematics of oceanic basalts: implication for mantle composition and processes. In: Saunders A, Norry M (eds) *Magmatism in the ocean basins*. *Geol Soc Lond Spec Publ* 42:313–345
- Thompson AB (1996) Fertility of crustal rocks during anatexis. *Trans R Soc Edinburgh Earth Sci* 87:1–10
- Tomomasini S, Davies GR (1997) Isotope disequilibrium during anatexis: a case study of contact melting, Sierra Nevada, California. *Earth Planet Sci Lett* 148:273–285
- Vielzeuf D, Holloway JR (1988) Experimental determination of the fluid-absent melting relations in the pelitic system. *Contrib Miner Petrol* 98:257–276
- Vielzeuf D, Montel JM (1994) Partial melting of metagreywackes; Part 1, fluid-absent experiments and phase relationships. *Contrib Miner Petrol* 117:375–393
- Whittington AG, Treloar PJ (2002) Crustal anatexis and its relation to the exhumation of collisional orogenic belts, with particular reference to the Himalaya. *Miner Mag* 66:53–91
- Wyllie PJ (1977) Crustal anatexis: an experimental review. *Tectonophysics* 43:41–71
- Zeng L (2003) Non-modal partial melting of metasedimentary pendants in the Southern Sierra Nevada and implications for the deep origin of within-pluton isotopic heterogeneity. PhD Thesis, California Institute of Technology, p 225
- Zeng L, Saleeby JB, Asimow P (2005a) Nd isotope disequilibrium during crustal anatexis: a record from the Goat Ranch migmatite complex, southern Sierra Nevada batholith, California. *Geology* 33:53–56
- Zeng L, Asimow P, Saleeby JB (2005b) Coupling of anatectic reactions and dissolution of accessory phases and the Sr and Nd isotope systematics of anatectic melts from a metasedimentary source. *Geochim Cosmochim Acta* 69:3671–3682